AIP Journal of Applied Physics

Selective metallization by seeded growth on patterned gold nanoparticle arrays

M. A. Raza, H. J. W. Zandvliet, B. Poelsema, and E. S. Kooij

Citation: Journal of Applied Physics **113**, 233510 (2013); doi: 10.1063/1.4811229
View online: http://dx.doi.org/10.1063/1.4811229
View Table of Contents: http://scitation.aip.org/content/aip/journal/jap/113/23?ver=pdfcov
Published by the AIP Publishing

Articles you may be interested in

Electroless deposition of metal nanoparticle clusters: Effect of pattern distance
J. Vac. Sci. Technol. B **32**, 031804 (2014); 10.1116/1.4870058

Modeling and numerical simulations of growth and morphologies of three dimensional aggregated silver films
J. Appl. Phys. **112**, 094310 (2012); 10.1063/1.4761993

Selective electroless coating of palladium nanoparticles on metallic single-walled carbon nanotube
Appl. Phys. Lett. **97**, 083101 (2010); 10.1063/1.3483615

Formation of ultrafine uniform gold nanoparticles by sputtering and redeposition
Appl. Phys. Lett. **94**, 133107 (2009); 10.1063/1.3111443

Metal pattern fabrication using the local electric field of a conducting atomic force microscope probe
J. Vac. Sci. Technol. A **15**, 1455 (1997); 10.1116/1.580561

Reuse of AIP Publishing content is subject to the terms at: https://publishing.aip.org/authors/rights-and-permissions. Download to IP: 130.89.45.232 On: Tue, 10 May 2016 07:25:49

JOURNAL OF APPLIED PHYSICS 113, 233510 (2013)

Selective metallization by seeded growth on patterned gold nanoparticle arrays

M. A. Raza,[1,2] H. J. W. Zandvliet,[1] B. Poelsema,[1] and E. S. Kooij[1,a)]
[1]*Physics of Interfaces and Nanomaterials, MESA+ Institute for Nanotechnology, University of Twente, P.O. Box 217, 7500AE Enschede, The Netherlands*
[2]*Centre of Excellence in Solid State Physics, University of the Punjab, QAC, Lahore 54590, Pakistan*

(Received 30 April 2013; accepted 30 May 2013; published online 19 June 2013)

We describe the selective metallization by electroless gold deposition on pre-patterned arrays of seed particles. In the first step, highly selective deposition of seeds (gold nanoparticles) on silicon oxide surfaces is achieved using pure water. In the second step, employing an electroless seeded growth process, the isolated nanoparticles are enlarged beyond the percolation threshold to deposit conducting metal structures. We obtain patterned gold films which exhibit macroscopic conductivity values approximately a factor of three lower than that of bulk gold. The surface morphology of the films has been characterized by scanning electron microscopy and spectroscopic ellipsometry. We discuss the different regimes as observed in morphological, electrical, and optical characterization in relation to each other. The free electron contribution to the optical spectra is analyzed in terms of the Drude model. Also, the formation of gold clusters during the growth process in the non-seeded area is described. © *2013 AIP Publishing LLC*. [http://dx.doi.org/10.1063/1.4811229]

I. INTRODUCTION

The stringent demands posed by modern technologies on ultra-large-scale-integration (ULSI) and microelectromechanical systems (MEMS) require high quality metal wirings. The choice of metal depends strongly on the dimension and precision in the selectivity of these interconnects to produce optimal electronic devices. Silver and gold are potential candidates to replace aluminum and copper in ULSI circuits.[1,2] Despite the fact that silver has the highest electrical conductivity of all metals, gold with its relatively high melting point, higher chemical stability, and larger electromigration resistance may well be a promising choice for ULSI multilevel interconnections, especially for sensitive electronic devices and in high frequency applications to limit signal noise and loss.[3] Furthermore, its good biocompatibility and electrochemical stability render it beneficial for application in, for example, biotransistors and bioelectronic devices.[4,5]

To fabricate devices for practical applications, one of the main goals is to achieve a high selectivity of metallization. Conventional metallization approaches include sputtering, vacuum evaporation, chemical/physical vapour deposition,[6,7] and electrochemical deposition.[8] The requirements imposed by vacuum setups, electrical apparatus, equipment maintenance, use of polluting chemicals for patterning, and waste of metal render these methods relatively expensive.

As an alternative, electroless metallization is inexpensive, easy in handling, environmental friendly due to the use of aqueous suspensions under ambient conditions, and well-developed in terms of metal layer quality. As such, it has become an attractive deposition technique for the microelectronics and semiconductor industries.[9,10] Moreover, using electroless plating it is possible to deposit a wide range of metals including noble metals, copper (Co), nickel (Ni), iron (Fe), and aluminum (Al).

In the electroless growth process a metal is deposited chemically from a solution which contains a reducing agent and an ionic metal complex as a precursor for deposition onto a catalyzed sample surface;[11,12] the autocatalytic redox process does not need an external current supply. Since only surface areas where the catalyst is present are metallized by this technique, it provides an ideal approach for selective metallization.

Prior to employing the electroless plating in this approach for selective metallization, a sufficiently dense patterning of catalysts, i.e., seed particles, is required to initiate the electroless reaction. Well-documented techniques to produce patterned nanoparticle layers include photolithography,[13–15] soft lithography including microcontact printing,[16,17] electron beam lithography,[18,19] dip-pen lithography,[20] scanning probe lithographic approaches,[21,22] nanoimprint lithography,[23] focused ion beam lithography,[24] and laser based patterning methods.[25–27] A special class of patterning methods with the capability to achieve feature sizes in the low nanometer range comprise controlled dewetting approaches in which surface tension-induced instabilities are employed. Ion beam or laser induced dewetting on prepatterned arrays[28,29] and/or on topographically patterned silicon substrates[30,31] has been described; in the latter, templating is attributed to the local curvature of the film over the topography. Related to the aforementioned approaches, a recently developed technique is referred to as template-confined dewetting.[32,33] After deposition of micropatterned metal arrays, thermal treatment induces dewetting to form nanoscale metal entities. Overall, despite their potentially huge impact on nanotechnology, in general, all the aforementioned approaches pose numerous disadvantages and limitations.

Photolithography, electron and ion beam lithography, as well as scanning probe lithographic techniques can achieve

a)Electronic mail: e.s.kooij@utwente.nl

 © 2013 AIP Publishing LLC

Reuse of AIP Publishing content is subject to the terms at: https://publishing.aip.org/authors/rights-and-permissions. Download to IP: 130.89.45.232 On: Tue, 10 May 2016 07:25:49

high resolution patterning.[22,23,34] However, relatively long processing times, the waste of materials during etching and recycling, the cost of fabrication, sophisticated equipment and maintenance, and the necessity for a cleanroom make these techniques relatively expensive. In addition, the use of irradiation and hazardous chemicals for developing resist films and etching limits their use in patterning nanoparticles or molecules with organic functionalities, since these chemicals may destroy the organic molecules and biological entities.[20,35–38] Although microcontact printing, which makes use of an elastomeric stamp, is a versatile, cost effective, and fast method, diffusion of ink on the substrate restricts its use for higher resolution patterning.[16] Dip-pen lithography using an atomic force microscope tip is effective for nanoscale patterning,[21] but due to the relatively low transfer efficiency, large scale patterning is not trivial.

Recently we have shown that pure water can be employed to selectively "defunctionalize" (3-mercaptopropyl)trimethoxysilane (MPTMS) coated surfaces, giving rise to spatial areas where gold nanoparticles do not adsorb during self-assembled formation of nanoparticle monolayers from solution.[39] A possible mechanism accounting for the absence of gold nanoparticles on water-treated (WT) areas was described in terms of a thin adsorbed water layer. Differences in electronegativities for the different entities (sulfur, oxygen, and hydrogen) suggest a hydrogen-like bonding between the water molecules and the thiol groups. The water layer effectively shields the thiol entities, inhibiting the attachment of gold nanoparticles. We found that this amazing role of water can be used as a fast, simple, and low cost tool enabling patterned deposition of nanoparticles on flat as well as microstructured surfaces.

Here we present the highly selective metallization of gold on silica substrates in a simple two-step method. As a first step selective patterning of gold nanoparticles is achieved by our aforementioned "water treatment" method.[39] In a subsequent step, these predeposited nanoparticles are used as seed particles for gold metallization by electroless growth. The metallization procedure is similar to previous work, in which we locally deposited silver by electroless growth on nanoparticle monolayers, which were patterned using microcontact printing.[40] Considering that we use MPTMS as a binding agent for our nanoparticles, which can also be used for other materials such as silver, copper, and platinum,[41] the method described here can, in principle, be extended for selective metallization by other materials.

II. EXPERIMENTAL DETAILS

A. Materials and substrate preparation

Hydrogen tetrachloroaurate ($HAuCl_4$, 99.999%), sodium citrate ($Na_3C_6H_5O_7$, 99%), hydroxylamine (NH_2OH, 50%), and MPTMS ($C_6H_{16}O_3SSi$, 97%) were obtained from Aldrich and used as received without any further purification. All other chemicals (sulfuric acid 97%, hydrogen peroxide 30%, 2-propanol, methanol, and ethanol) were of analytical grade from Merck. Water with a resistivity of 18.2 MΩcm, purified in a Milli-Q system, was used for the preparation of aqueous solutions and for other experimental purposes.

Substrates ($1 \times 1\,cm^2$ pieces) were diced from polished silicon wafers by scratching the edge of a thin Si(100) wafer with a diamond scribe on a soft surface. The silicon substrates are covered with a 1.8 ± 0.1nm native oxide layer (as measured by spectroscopic ellipsometry). After ultrasonic cleaning in methanol for 15 min, samples were immersed in piranha solution (mixture of sulfuric acid and hydrogen peroxide $H_2SO_4/H_2O_2 = 3{:}1$ (v/v)) for 30 min and rinsed thoroughly with purified water and dried in a N_2 flow.

The cleaned substrates were functionalized with MPTMS by immersion in a 12% (v/v) solution in 2-propanol.[42] All substrates were immersed in this solution for one day at room temperature, rinsed with pure propanol, and annealed at 110 °C for 10 min. The thickness of the MPTMS self-assembled monolayers (SAM), as determined by ellipsometry, was 0.65 ± 0.1nm, close to the theoretical value of the length of MPTMS molecules (0.77 nm).[43] To assess the quality and reproducibility of our MPTMS monolayers, the water contact angle was measured on the MPTMS treated substrates by using the sessile drop method under ambient conditions at room temperature; in all cases the contact angle amounted to a value of $60 \pm 2°$, which is close to that reported for highly organized MPTMS SAMs.[44]

B. Patterned gold nanoparticle deposition

Colloidal gold nanoparticles with a diameter of 50 nm in suspensions were prepared in two steps. First, 13 nm gold nanoparticles were prepared, which were then used as seed particles for enlargement by citrate reduction; details are given elsewhere.[39]

Patterned deposition of gold nanoparticles was performed as described in our previous work,[39] where we have described the deactivation of the thiol functionalisation by the formation of a capping water layers. Briefly, the MPTMS derivatized samples were locally treated with pure water at room temperature in open air for a few minutes (typically 1–5 min). In the water-treated areas, the MPTMS layer is deactivated, and gold nanoparticles do not adsorb on these specific areas. In the drying process using a N_2 flow, most of the liquid is blown off the surface.

To achieve irreversible adsorption of the gold nanoparticles on MPTMS-coated substrates, the samples were immersed into the gold colloidal suspensions for 12–15 h (overnight) at room temperature, followed by thorough rinsing with pure water and drying in a N_2 flow.

C. Seeded gold growth by electroless plating

The irreversibly adsorbed gold nanoparticles act as seeds for the electroless deposition of gold. Electroless plating on patterned seeds was carried out following a previously reported method.[45,46] The aqueous solution of 1 mM $HAuCl_4$ and 1 mM NH_2OH in equal ratio (1:1) was prepared under vigorous agitation (using a magnetic stirrer) to initiate growth. After a few seconds (10–20 s), the magnetic stirrer was taken out, and the solution bath was placed on an orbital shaker before immersing samples with patterned seed particles in the solution. Electroless metallization was carried out on the orbital shaker at 100 rpm at room temperature

Reuse of AIP Publishing content is subject to the terms at: https://publishing.aip.org/authors/rights-and-permissions. Download to IP: 130.89.45.232 On: Tue, 10 May 2016 07:25:49

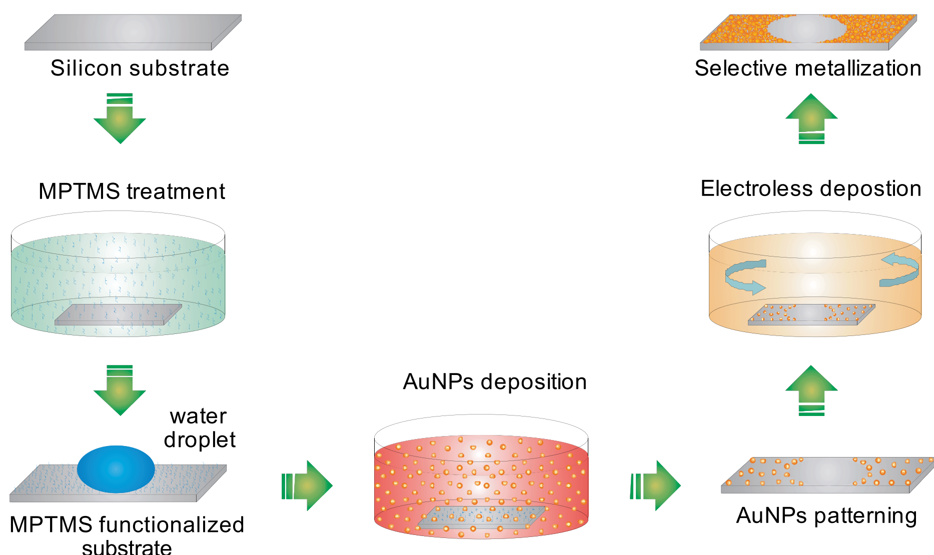

FIG. 1. Schematic illustration of the selective gold metallization. MPTMS coated substrates are selectively treated with pure water followed by gold nanoparticle deposition to obtain patterned gold arrays, which act as seeds for subsequent electroless plating.

(22 °C) for 30 min, at 5 min intervals. After each coating cycle, substrates were rinsed with pure water and dried in a N_2 flow before immersing them for the next cycle.

D. Surface characterization

The surface morphology of the prepared samples was assessed by scanning electron microscopy (SEM; HR-LEO 1550 FEF). Typical acceleration voltages of 1–2 keV were used; such low voltages allow imaging of non-conductive samples without the necessity of a thin metal coating. The imaging voltages do not give rise to any discernable modification of the morphology during the time needed to acquire the images.

Contact angle measurements were performed using the sessile drop method on a Dataphysics OCA15+ goniometer under ambient conditions at room temperature. A variable angle spectroscopic ellipsometer (VASE, J.A. Woollam) was used to determine the thickness of the applied films, to verify the presence of gold nanoparticles and to investigate optical properties after electroless growth cycles. The films were investigated in the photon energy range 0.8–4.5 eV, at a fixed incidence angle of 70° with respect to the surface normal. The macroscopic conductivity of the layers after different gold metallization cycles was determined by four-point probe method (Metrology Matheson 4-point measurement) while the film thickness was assessed using a surface profiler (Metrology VEECO Dektak 8.0).

III. SELECTIVE METALLIZATION PROCEDURE

In Fig. 1 a schematic representation of the procedure to achieve highly selective gold metallization is illustrated. In the first step clean silicon substrates with a thin native oxide layer are functionalized with MPTMS via the immersion method, therewith inducing a high affinity for irreversible deposition of gold nanoparticles. Subsequently, the MPTMS-derivatized samples are selectively brought into contact with pure water to defunctionalize the surface. Next, nanoparticles are deposited by immersing the samples into citrate-stabilized nanocolloidal gold suspension. This gives rise to patterned arrays of gold nanoparticles. Up to this point, the procedure is identical to that described in our previous work.[39]

The patterned gold arrays act as seeds to the subsequent metallization. The patterned substrates are immersed into an electroless gold plating solution at room temperature on an orbital shaker for a specific time, typically 5–30 min. In Fig. 2 photographic images (from a top-view camera) of the sample at different stages during the procedure are shown. Water treatment after MPTMS functionalization using mm-sized droplets (left) is followed by spatially patterned nanoparticle adsorption (middle) after which the samples are selectively metallized by electroless gold deposition (right). The surface areas which have been in contact with water can clearly be identified as circular spots on the sample after nanoparticle deposition and subsequent gold metallization. The enhanced contrast after electroless deposition, primarily due to the higher reflectivity of the gold in the non-WT regions, arises from the thicker and denser metallic gold layer after prolonged metallization. Details of the optical properties will be discussed in Sec. V.

A macroscopic overview of a patterned substrate and microscopic images of the WT and non-WT regions after

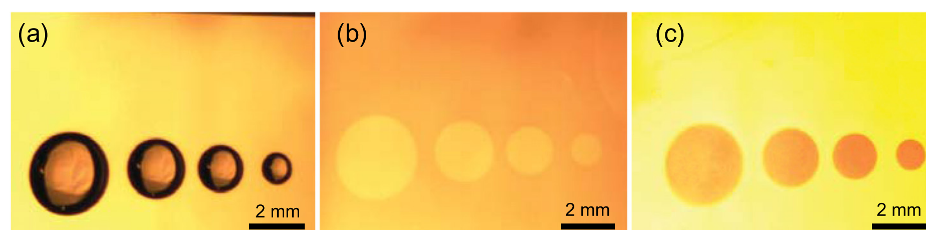

FIG. 2. Top-view images showing a substrate (a) during water treatment with droplets of different sizes, (b) after deposition of gold nanoparticles, and (c) after electroless metallization. The colour scheme in different images does not exactly reflect the true colours.

Reuse of AIP Publishing content is subject to the terms at: https://publishing.aip.org/authors/rights-and-permissions. Download to IP: 130.89.45.232 On: Tue, 10 May 2016 07:25:49

adsorption of 50 nm gold nanoparticles are shown in Fig. 3. The circular spot in the SEM image (bottom left) corresponds to the area of the substrate that was in contact with the droplet during water treatment. A sharp discontinuity in contrast clearly separates the WT and non-WT areas. The darker shade in the centre of the spot arises from charging of the exposed oxide by electrons. Enlargements are shown for three different regions corresponding to the non-WT area (top right), the WT area (bottom right), and the boundary region (top left).

Close inspection of the boundary separating WT and non-WT regions, as shown in upper left part of Fig. 3, reveals that gold nanoparticles are only deposited on the non-WT surface, while on the WT area attachment of nanoparticles is very effectively inhibited. The latter is also shown in the enlarged image of the WT region (bottom right). Surprisingly, not even a single gold particle can be discerned in this area, substantiating the excellent level of selectivity induced by the water treatment due to effective defunctionalization of the MPTMS monolayer, as discussed previously.[39]

In the untreated area (top right) a homogeneous distribution of irreversibly deposited nanoparticles is observed. The exposed thiol groups of the MPTMS molecules induce a high affinity for gold nanoparticles, which results in the irreversible attachment to the surface. Due to stabilization of the nanoparticle suspension by citrate adsorption, the nanoparticle surface becomes negatively charged. Upon approaching each other, particles in suspension experience a net repulsion. The spatial extent of this repulsive interaction also gives rise to a minimum interparticle spacing between adsorbed nanoparticles on the surface.[47] In contrast of this short-ranged organization, there is no long-range interaction yielding a random spatial distribution, as can be seen in the SEM image (top right in Fig. 3).

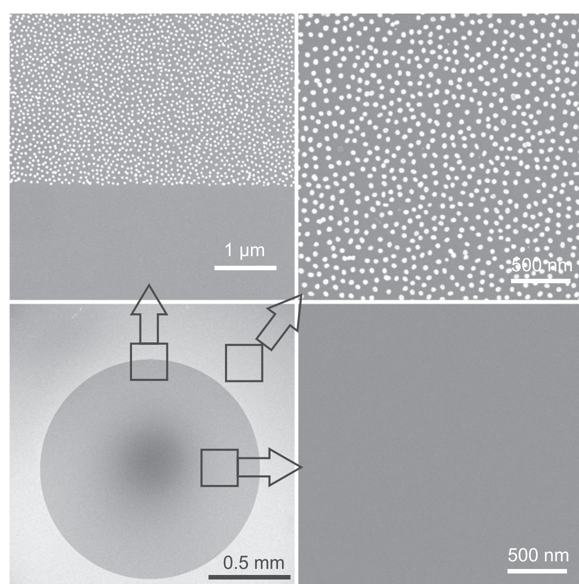

FIG. 3. SEM images showing the distribution of gold nanoparticles in three different regions after adsorption: (bottom right) WT area, (top right) non-WT area, and (top left) the boundary between both regions. The large scale overview (bottom left) shows the entire circular area, which was in contact with the water droplet.

The morphology of pre-patterned samples after seeded gold growth is shown in Fig. 4. Again, a macroscopic overview of the complete circular region, which was treated with water prior to nanoparticles deposition, is shown together with enlargements of different regions. In the large scale image the contrast between WT and non-WT areas is more pronounced as compared to that before seeded growth (Fig. 3, bottom left image). The boundary between WT and non-WT regions (shown in the top left image) appears to be very sharp, clearly distinguishing between areas where predeposited nanoparticles were present and where they were absent. Apparently, the gold metallization is also highly selective, leading to a thick gold film only in the non-WT section where gold seed particles are present. The morphology of the thick metallic layer in the non-WT area, i.e., outside the circular spot, is characterized by a large number of densely packed grains of different sizes.

Owing to the absence of nanoparticles in the WT area such a metallic layer could not develop (bottom right). However, within the circular spot, i.e., the WT area, randomly distributed islands of different sizes in the low micrometer range can be observed as white spots in the SEM images. Our initial assumption was that these relatively large clusters form in solution and subsequently sediment onto the surface under the influence of gravity. However, changing the orientation of the substrate during seeded growth, even upside down, reveals that the clusters are still formed in the WT regions. Further details on the evolution of the morphology with seeded growth time are discussed in Sec. IV.

IV. MORPHOLOGY EVOLUTION DURING SEEDED GROWTH

The temporal evolution of the morphology of the metallic layer during seeded growth of gold preferentially on the

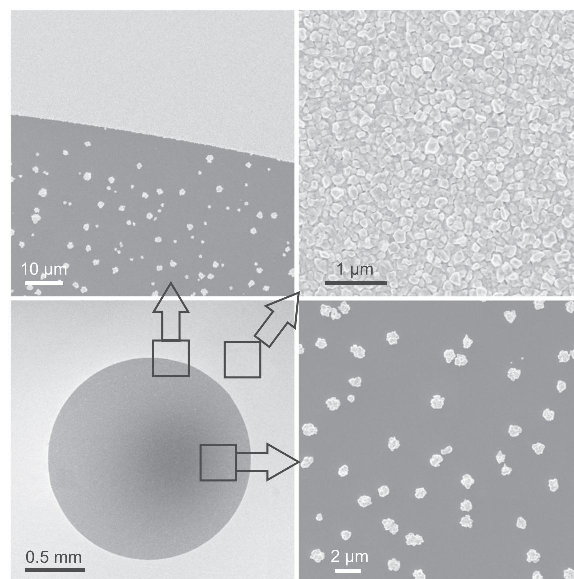

FIG. 4. SEM images showing the morphology in three different regions after electroless deposition for 30 min on the patterned gold nanoparticle arrays: (top right) non-WT area, (bottom right) WT area, and (top left) the boundary between both regions. The large scale overview (bottom left) shows the complete circular area, which was in contact with the water droplet prior to deposition of nanoparticles.

Reuse of AIP Publishing content is subject to the terms at: https://publishing.aip.org/authors/rights-and-permissions. Download to IP: 130.89.45.232 On: Tue, 10 May 2016 07:25:49

immobilized gold nanoparticles is illustrated by the SEM images in Fig. 5. Electroless deposition times were varied up to 30 min. Gold ions (Au^{3+}) are reduced by NH_2OH, a process catalysed by the pre-deposited gold seed particles. The images are acquired on the same samples as used for the electrical conductivity and ellipsometry experiments, which will be presented in Sec. V. The images in the right column show the boundary between WT and non-WT regions, while

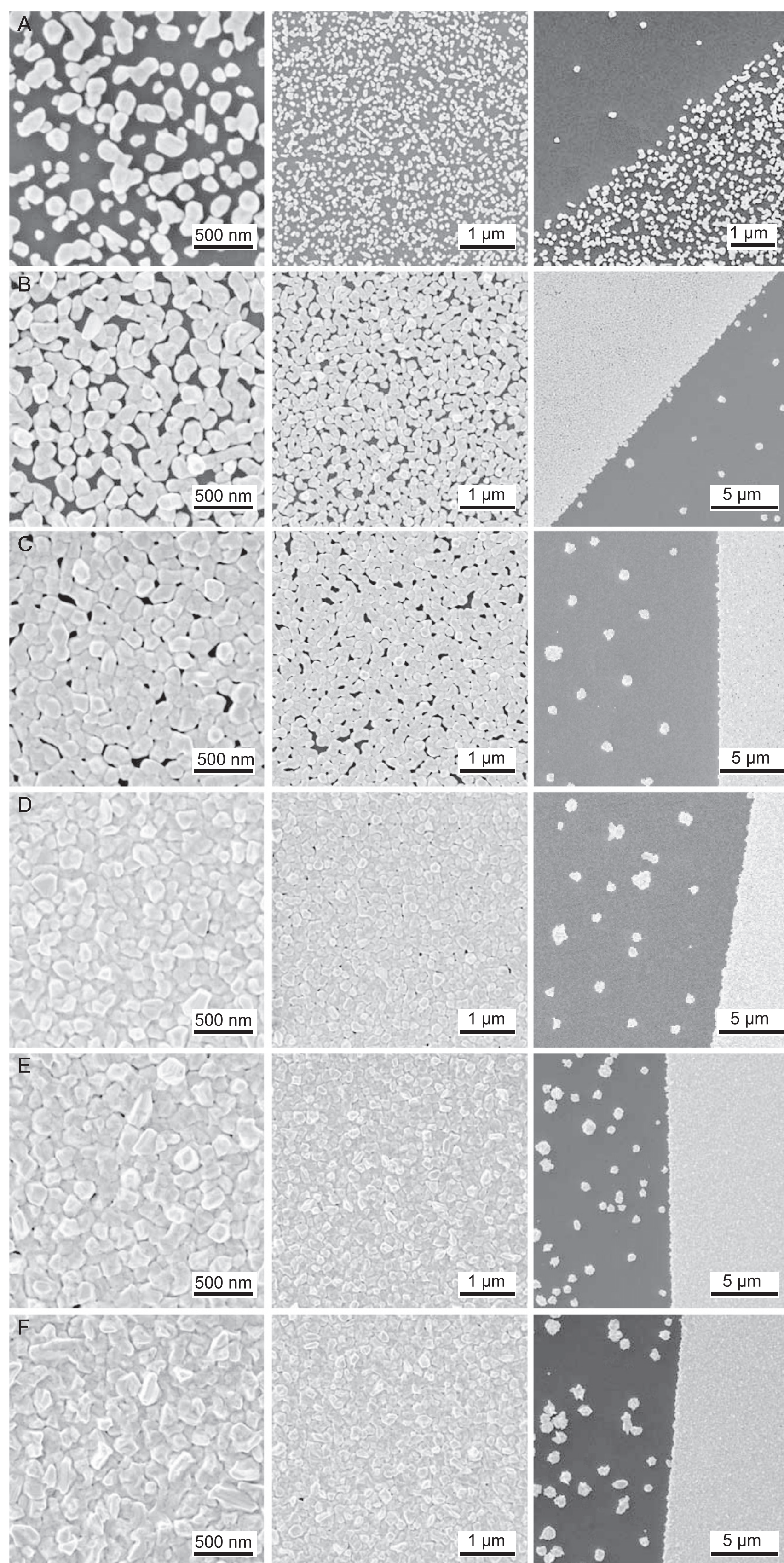

FIG. 5. SEM images showing the morphology of the samples for different electroless plating times: panel A (5 min), panel B (10 min), panel C (15 min), panel D (20 min), panel E (25 min), panel F (30 min). The right column depicts the boundary between seeded (non-WT) and seedless (WT) parts, while the middle and left columns show the seeded area, at different levels of magnification.

Reuse of AIP Publishing content is subject to the terms at: https://publishing.aip.org/authors/rights-and-permissions. Download to IP: 130.89.45.232 On: Tue, 10 May 2016 07:25:49

the middle column depicts the development of the metal film in the non-WT areas. Finally, the left column illustrates magnified views, revealing the polycrystalline nature of the metallic layer.

The effect of the initial electroless plating for 5 min is demonstrated in panel A of Fig. 5. Reduction of Au^{3+} ions by NH_2OH seems to occur preferentially on the predeposited spherical seed particles. Individual particles grow larger in size but also appear to develop into more irregular shapes. Furthermore, the formation of small islands encapsulating multiple particles is initiated, but the fusion of many particles is very rare in this phase (left image, panel A). The island density remains approximately constant, since nucleation of new entities does not occur; similar results were described for gold deposition by sputtering on predeposited palladium islands.[48] The sizes of these islands vary from about 100 nm to 500 nm. Most of the islands, typically 90%-95%, as well as individual enlarged particles, are still well separated (middle image), in line with the negligible conductivity obtained in electrical measurements.

After 10 min of electroless coating (panel B), the existing islands appear to become progressively larger, and coalescence between the islands occurs frequently. Between the islands, relatively large gaps are still observed. Due to this "fusion" of individual metallic entities, there is barely a continuous connection over long distances across the sample surface. Nevertheless, the fact that a percolation threshold is reached is confirmed by the conductivity measurements, which show small but measureable values. Close examination of the surface morphology suggests that some crystals grow faster in height than others (left image, panel B), therewith enhancing the roughness of the deposited structure.

With progressive fusion of the deposited nanoparticles after 15 min, the original nanostructures are completely obscured (middle image, panel C); only a few scattered vacancy islands in the film can still be seen, which indicates an incomplete coalescence of large islands at this stage. The electrical measurements reveal that conductivity increases as a result of additional gold deposited, increasing the overall thickness and eventually filling the voids in the metal film.

Images of thick gold films obtained after prolonged electroless deposition for 20, 25, and 30 min are collected in panels D, E, and F, respectively. All films on seeded areas exhibit large-scale particle fusion producing compact gold layers, free from any gaps. By increasing the deposition time from 20 to 30 min, more gold is deposited on the existing coalesced islands, enlarging them in size and shape and thereby enhancing the roughness as well as overall thickness of the films. In the boundary region (images in the right column), a clear separation is observed defined by the sharp division of electroless plating on seeded (non-WT) and seedless (WT) areas.

During the electroless plating procedure, gold is not only deposited in the non-WT areas where a large density of nanoparticles is present but also in the seedless WT part of the surface, where clusters are clearly observed (right images in Fig. 5); we assume these clusters to consist of gold. With increasing electroless growth time, the number of gold clusters appears to increase, while their average size also rises.

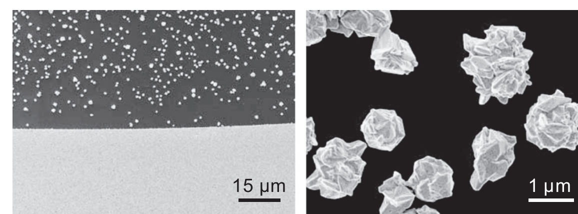

FIG. 6. SEM images revealing the distribution (left) and morphology (right) of the clusters on the WT part of a sample after 30 min electroless deposition.

In Fig. 6 (left) the distribution of deposited islands on the seedless (WT) part is shown. Although the spatial distribution appears to be random, the results in Figs. 5 and 6 seem to suggest that their density near the boundary is slightly lower.

The right image shows a zoom in of the clusters, revealing their irregular shape. Some of them have a flower-like shape, while the smaller ones have less protrusions. With increasing electroless plating time, the gold clusters increase in size. The size range as a function of deposition time is summarized in Table I. For the shortest times, the clusters are still in the 100–200 nm range, but after prolonged growth they can reach diameters as large as 2.5 μm. From the fact that the gold clusters are formed, we conclude that despite the absence of gold seed particles in the WT area, there are nucleation sites where gold growth is initiated. However, in sharp contrast to the seeded areas, the gold clusters do not coalesce into interconnected, conducting superstructures.

V. ELECTRICAL AND OPTICAL CHARACTERISATION

To verify the continuity and therewith the conductivity of the electroless grown gold films at specific stages, four-point probe electrical measurements have been carried out at room temperature. The results are summarized in Table II and graphically represented in Fig. 7. The thickness of the deposited films as determined using a profilometer versus deposition time is shown in Fig. 7(a). The thickness curve can be divided into three distinct regimes. The first region for deposition times up to 10 min corresponds to the images in Fig. 5 where the individual gold particles only grow in size without forming a continuous layer; during this time the island density remains constant.[48] The second regime between 10 and 20 min shows a slower increase of thickness with time. In this regime, the isolated gold islands coalesce as a result of additional gold that is deposited, and the voids in the layer are subsequently filled. In the last regime for deposition times exceeding 20 min the film grows only in thickness and appears to become rougher with time.

TABLE I. Typical size range of metallic clusters on the seedless WT area for different deposition times.

Deposition time (min)	Cluster size range (nm)
5	100–200
10	300–800
15	500–1500
20	600–2000
25	650–2200
30	800–2500

Reuse of AIP Publishing content is subject to the terms at: https://publishing.aip.org/authors/rights-and-permissions. Download to IP: 130.89.45.232 On: Tue, 10 May 2016 07:25:49

TABLE II. Measured sheet resistance, thickness, and calculated conductivity of deposited gold films on the seeded, non-WT part as a function of electroless plating time.

Deposition time (min)	Sheet resistance (mΩ)	Film thickness (nm)	Conductivity (10^6 S/m)
5	∞	100.00	0
10	6351.05	145.23	1.08
15	2187.99	153.74	3.02
20	441.22	172.82	13.12
25	283.75	213.43	16.53
30	244.62	256.05	15.97

The aforementioned three regimes can also be identified in the plot of the conductivity as a function of deposition time as shown in Fig. 7(b). Up to 10 min electroless growth, there is no continuous percolating current path across the surface (see also Fig. 5). As such, there is no conductivity. In region II from 10 to 20 min deposition time the islands start to coalesce, while the voids are progressively filled resulting in a more compact metallic layer. Owing to more gold being deposited, with time the conductivity increases toward its saturation value. In the saturation regime III for times exceeding 20 min the film thickness grows more or less homogeneously. The sheet resistance decreases primarily due to the thickness increase, while the conductivity starts to saturate at a value of approximately $16 \times 10^6 \mathrm{S/m}$.

This saturation value of the conductivity for prolonged gold deposition is approximately a factor of 2.8 lower than the bulk conductivity of gold,[49] which amounts to $45.25 \times 10^6 \mathrm{S/m}$. The fact that our films, which appear to be fully developed, exhibit such relatively low conductivity values may well be due to increased roughness, to voids built into the layer (not visible in the top-view SEM images), and to the fact that there are substantially more grain boundaries in the deposited film.

Optical characterization of the metal films at various stages of electroless growth is performed by employing spectroscopic ellipsometry. In Fig. 8 *ex situ* ellipsometry spectra are shown of deposited films on seeded (non-WT) parts of the surface for different deposition times. The sample morphology as revealed by SEM images corresponding to these spectra has been described in relation to Fig. 5. The ellipsometry spectrum (red line) of a monolayer of 50 nm gold nanoparticles on silicon oxide prior to electroless deposition shows a characteristic feature near 2.3 eV. The pronounced minimum in Δ corresponds to the surface plasmon resonance of the gold nanoparticles.[51] Moreover, at energies above 3.2 eV spectral features of the silicon substrate, i.e., through the semi-transparent particulate metal layer, are still visible.

Already after 5 min electroless plating, the spectrum changes markedly. The characteristic plasmon resonance feature near 2.3 eV becomes less prominent and shifts to lower energies. We ascribe the spectral changes to the enlargement of the individual particles and the formation of larger islands with irregular shapes. By further increasing the

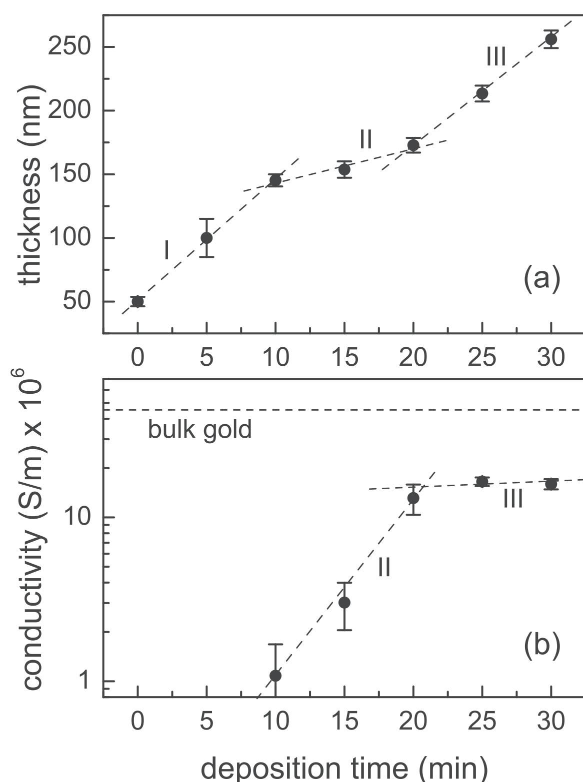

FIG. 7. Measured thickness (a) and conductivity (b) of electroless grown gold films as a function of plating time. The dashed lines are a guide to the eye; the dotted line in (b) represents the conductivity value for bulk gold.

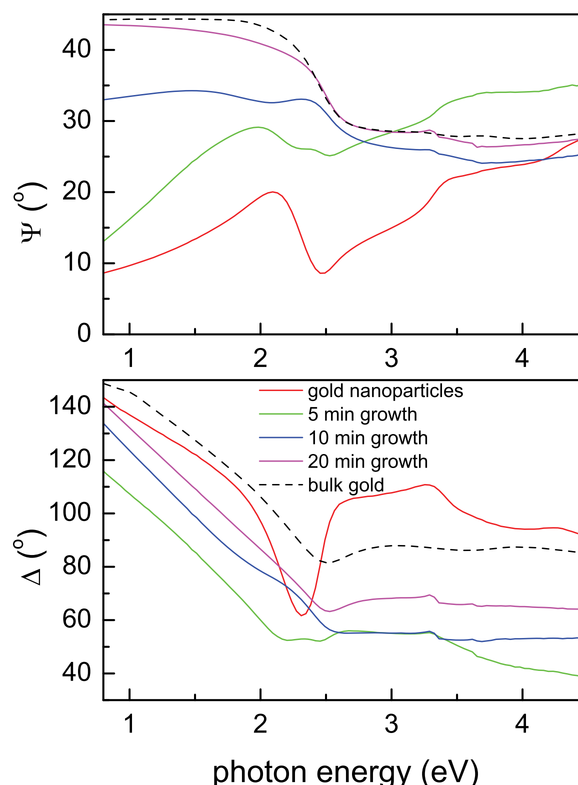

FIG. 8. Ellipsometry spectra, i.e., Ψ and Δ as a function of photon energy, of electroless deposited gold films on oxide coated silicon substrates for different plating times. Red lines correspond to samples with only gold nanoparticles, while the green, blue, and magenta spectra correspond to electroless deposition times of 5 min, 10 min, and 20 min, respectively. The black dashed lines represent calculated spectra for bulk gold.

Reuse of AIP Publishing content is subject to the terms at: https://publishing.aip.org/authors/rights-and-permissions. Download to IP: 130.89.45.232 On: Tue, 10 May 2016 07:25:49

deposition time the spectra develop into a response which shows distinct similarities with that of bulk gold.

As a comparison, ellipsometry spectra for bulk gold, as calculated using the dielectric function as tabulated by Johnson and Christy,[50] are represented by the dashed lines. For energies below 2.3 eV the high reflectivity of gold gives rise to a value for Ψ of 45°. Near 2.3 eV a drop in Ψ is observed both in the calculated and measured spectra. This indicates that indeed the developed metal layer is continuous and bulk like. The variation of Δ with photon energy after prolonged deposition exhibits a very similar curve as the bulk gold calculation, but an offset is observed. This offset does not decrease for even longer deposition times. The discrepancy can be reasoned by considering the surface roughness of the film. In fact, the slightly lower Ψ values between 1.0 eV and 2.0 eV in the experimental spectra are also due to roughness, combined with voids in the layer.

On the basis of the ellipsometry spectra shown in Fig. 8 we can determine pseudo-dielectric functions by inversion of the ellipsometric parameters. To do this we assume the sample to be a two-phase system, i.e., only a substrate and the ambient. The resulting real and imaginary parts of the dielectric function for different electroless deposition times are shown in Fig. 9. Prior to the gold deposition, the dielectric function is dominated by 50 nm AuNPs. Moreover, the ellipsometry spectra are due to reflection from the gold nanoparticles but also from the oxide-coated silicon substrate. As such, a simple quantitative analysis of this dielectric function is not possible.[51,52]

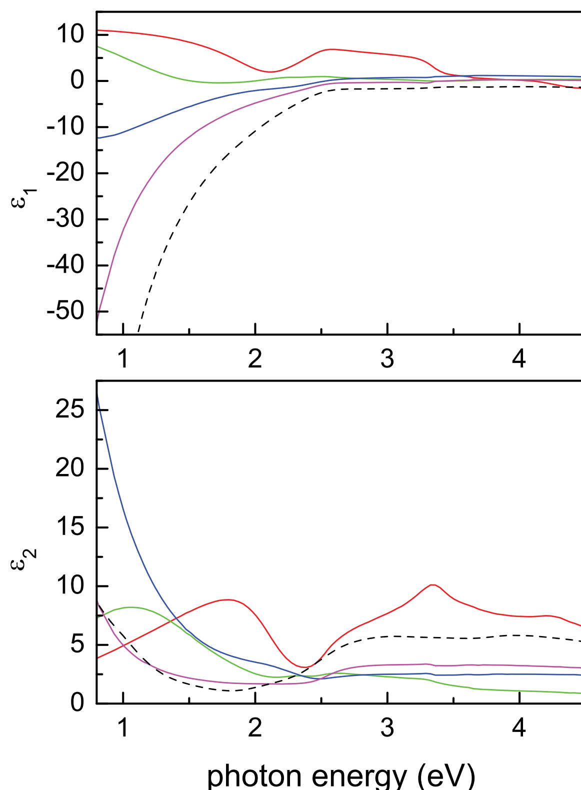

FIG. 9. Real (top) and imaginary (bottom) parts of the pseudo-dielectric functions before electroless gold deposition (red line) and after gold growth for 5 min (green), 10 min (blue), and 20 min (magenta), acquired by direct inversion of the spectra in Fig. 8. The dashed lines represent the bulk dielectric function as tabulated by Johnson and Christy.[50]

Nevertheless, as discussed by Oates *et al.*,[53,54] the pseudo-dielectric functions can be used to determine the percolation threshold of a growing metal film, i.e., the stage at which the film becomes continuous to such an extent that macroscopic current can be conducted. On the basis of their experiments on silver and titanium layers on oxide substrates, they suggest that when the real part of the dielectric function becomes negative in the low energy range, i.e., the infrared, this can be used as an indication of the transition from a nonconducting island film to an interconnected metal film. If we apply their model to our data, as shown in Fig. 9, to predict the percolation threshold, we obtain realistic results. The spectra of bare gold nanoparticles and after 5 min growth, the real part of the dielectric function is positive at the energies below 1.5 eV, while the gold film is nonconductive as shown in Fig. 7(b). For electroless plating times of 10 min and longer, the real part of the dielectric function in the infrared shifts from positive to negative, in good agreement with the finite, measurable conductivity values (Fig. 7). Of course, the method by Oates *et al.* provides only a rough estimate since the dielectric functions were only determined down to an energy of 0.8 eV. Nevertheless, we observe very reasonable agreement.

Upon prolonged deposition of gold by electroless growth, characteristic features related to free electrons in the film appear in the pseudo-dielectric function. Such Drude-like free electron behavior is characterized by a strong decrease of the real part for smaller energies and a distinct rise of the imaginary part. The dielectric function ε as a function of frequency ω is represented by

$$\varepsilon = \varepsilon_\infty - \frac{\omega_p^2}{\omega^2 - i\omega\Gamma}, \tag{1}$$

where the offset ε_∞ takes into account the contribution of interband transitions at higher energies. The electron relaxation rate $\Gamma = 1/\tau_D$ is the inverse of the electron scattering time τ_D, and $\omega_p = \sqrt{Ne^2/\varepsilon_0 m^*}$ is the plasma frequency with N the electron density, e the electron charge, and m^* the effective electron mass. For small relaxation rates, i.e., $\Gamma \ll \omega$, the real and imaginary parts of the dielectric function in Eq. (1) can be approximated as

$$\mathrm{Re}(\varepsilon) = \varepsilon_\infty - \frac{\omega_p^2}{\omega^2}, \tag{2a}$$

$$\mathrm{Im}(\varepsilon) = \frac{\omega_p^2 \Gamma}{\omega^3}. \tag{2b}$$

In Fig. 10 we show the results of fitting (Eqs. (1), (2a), and (2b)) to the pseudo-dielectric after 20 min gold deposition. Obviously, only at low frequencies ω there is good agreement, since at energies $\hbar\omega \gtrsim 1$eV interband transitions become important. From the fit results we obtain $\varepsilon_\infty = 5$, $\hbar\omega_p = 6.1$ eV, and $\tau_D = 5.5$ fs. Comparison of the exact Drude expression of Eq. (1) to the approximation in Eq. (2) (solid and dashed lines in Fig. 10) confirms the validity of the small relaxation rate approximation in the energy range accessible in our experiments.

Reuse of AIP Publishing content is subject to the terms at: https://publishing.aip.org/authors/rights-and-permissions. Download to IP: 130.89.45.232 On: Tue, 10 May 2016 07:25:49

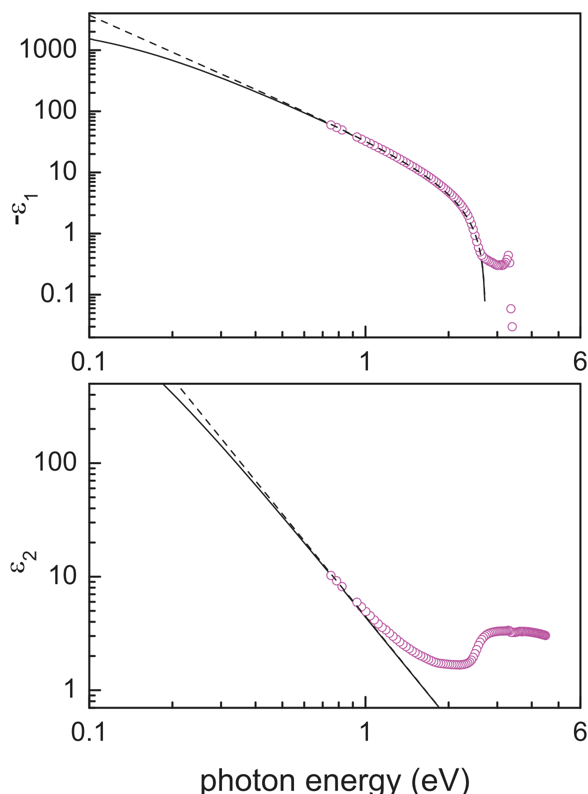

FIG. 10. Comparison of the pseudo-dielectric function after 20 min electroless growth (magenta symbols; see also Fig. 9) to calculations using the Drude model (solid line; Eq. (1)) and the approximation for negligible scattering rates (dashed lines; Eq. (2)). Log-log plots of $-\varepsilon_1$ and ε_2 are shown in the top and bottom panels, respectively.

We can now compare our results to established data for bulk gold as reported in literature. Recently, a detailed analysis of the optical properties of gold has been described by Olmon *et al.* in relation to previous reports on the gold dielectric function.[55] From a fit of their ellipsometry spectra to the Drude model they obtained an electron relaxation time $\tau_D = 14$ fs and plasma energy $\hbar\omega_p = 8.45$ eV. The lower value for the plasma frequency in our results is most likely related to a smaller density of electrons participating in the electronic processes, due to voids and the many grain boundaries in the film. In good agreement with the approximately three times smaller electrical conductivity in our films as compared to bulk gold, the relaxation time τ_D is also 2.5 times lower. Owing to significant scattering of the free electrons at surface roughness features as well as the large density of grain boundaries,[56] the dielectric functions of our fully developed film still deviate from the bulk values. Finally, using the scattering time with the Fermi velocity in gold $v_F = 1.4 \times 10^6$ m/s, we obtain a mean free path $\tau_D \cdot v_F \approx 7.7$ nm. This value is much smaller than the grain dimensions observed in Fig. 5, most likely due to defects and other scattering centres which are not resolved in these images.

VI. CONCLUSIONS

We have demonstrated a novel method to achieve selective gold metallization, in which gold nanoparticles are first selectively adsorbed on silicon oxide surfaces. Patterning was achieved by selectively deactivating the surface functionalization using pure water. The nanoparticles act as seeds to selectively initiate seeded growth by an electroless plating process. Electroless deposition for different time intervals was carried out to identify the percolated threshold. Electron microscopy images reveal that by increasing the deposition time the nanoparticles first grow into larger isolated islands via particle fusion. Subsequently, coalescence among islands leads to a percolated network. For prolonged deposition, the gold film becomes more compact due to filling of the voids in the layer, while the overall thickness increases. After passing the percolated threshold, the conductivity of the deposited films increases with increasing deposition time and saturates after approximately 20 min. Due to roughness and a high density of grain boundaries, the conductivity value of our deposited films remains lower than that of bulk gold by approximately a factor of three. Optical properties are assessed by means of spectroscopic ellipsometry. We have shown that the appearance of a clear Drude-like contribution in the dielectric function of the growing metal layer agrees well with the electrical measurements. On the WT areas where seed particles are completely absent, the formation of irregular flower-like gold clusters was observed. Although the exact mechanism for the formation of these clusters is not clear, we assume they nucleate at exposed thiol-groups on the non-seeded areas during the electroless growth. However, the clusters do not coalesce to form an interconnected layer and as such did not exhibit a measurable conductivity.

ACKNOWLEDGMENTS

The authors thank Naveed Kazmi (University of Twente) for performing the four-point probe measurements and are grateful for helpful discussions. We gratefully acknowledge the support by MicroNed, a consortium to nurture micro-systems technology in The Netherlands. M. A. Raza acknowledges support from the Higher Education Commission in Pakistan.

[1]C.-H. Hsu, M.-C. Yeh, K.-L. Lo, and L.-J. Chen, Langmuir **23**, 12111 (2007).
[2]C. Carraro, L. Magagnin, and R. Maboudian, Electrochim. Acta **47**, 2583 (2002).
[3]K. Mikagi, T. Homma, T. Katoh, K. Tsunenari, and Y. Murao, in *IEEE Proceedings of Sixth International VLSI Multilevel Interconnection Conference, 1989* (IEEE, 1989), pp. 33–39.
[4]J. Xie, Y. Miao, J. Shih, Q. He, J. Liu, Y. C. Tai, and T. D. Terry, Anal. Chem. **76**, 3756 (2004).
[5]S. H. Cho, S. H. Kim, J. G. Lee, and N. E. Lee, Microelectron. Eng. **77**, 116 (2005).
[6]P. van Zant, *Microchip Fabrication: A Practical Guide to Semiconductor Processing* (McGraw-Hill Professional Publishing, New York, 2000).
[7]M. Datta, T. Osaka, and J. W. Schultze, *Microelectronic Packaging* (CRC Press, Boca Raton, 2005).
[8]Z. M. Hu and T. Ritzdorf, J. Electrochem. Soc. **153**, C467 (2006).
[9]Y. Shacham-Diamand, A. Inberg, Y. Sverdlov, and N. Croitoru, J. Electrochem. Soc. **147**, 3345 (2000).
[10]Y. Okinaka and T. Osaka, *in Advances in Electrochemical Science and Engineering*, edited by H. Gerischer and C. W. Tobias (VCH, Weinheim, Germany, 1994), Vol. 3, p. 58.
[11]D. Zabetakis and W. J. Dressick, ACS Appl. Mater. Interfaces **1**, 4 (2009).
[12]G. O. Mallory, in *Electroless Plating: Fundamentals and Applications*, edited by G. O. Mallory and J. B. Hajdu (American Electroplaters and Surface Finishers Society, Orlando, FL, 1990), pp. 1–56.

Reuse of AIP Publishing content is subject to the terms at: https://publishing.aip.org/authors/rights-and-permissions. Download to IP: 130.89.45.232 On: Tue, 10 May 2016 07:25:49

[13]C. S. Dulcey, J. H. Georger, Jr., V. Krauthamer, D. A. Stenger, T. L. Fare, and J. M. Calvert, Science **252**, 551 (1991).
[14]C. W. Gwyn, R. Stulen, D. Sweeney, and D. Attwood, J. Vac. Sci. Technol. B **16**, 3142 (1998).
[15]T. Ito and S. Okazaki, Nature (London) **406**, 1027 (2000).
[16]N. L. Jeon, K. Finnie, K. Branshaw, and R. G. Nuzzo, Langmuir **13**, 3382 (1997).
[17]J. Zhang and B. Yang, Adv. Funct. Mater. **20**, 3411 (2010).
[18]D. W. Carr, M. J. Lercel, C. S. Whelan, H. G. Craighead, K. Seshadri, and D. L. Allara, J. Vac. Sci. Technol. A **15**, 1446 (1997).
[19]M. J. Lercel, R. C. Tiberio, P. F. Chapman, H. G. Craighead, C. W. Sheen, A. N. Parikh, and D. L. Allara, J. Vac. Sci. Technol. B **11**, 2823 (1993).
[20]R. D. Piner, J. Zhu, F. Xu, S. Hong, and C. A. Mirkin, Science **283**, 661 (1999).
[21]D. S. Ginger, H. Zhang, and C. A. Mirkin, Angew. Chem., Int. Ed. **43**, 30 (2004).
[22]R. Maoz, R. Frydman, S. R. Cohen, and J. Sagiv, Adv. Mater. **12**, 424 (2000).
[23]P. Maury, M. Péter, V. Mahalingam, D. N. Reinhoudt, and J. Huskens, Adv. Funct. Mater. **15**, 451 (2005).
[24]G. Gillen, S. Wight, J. Bennett, and M. J. Tarlov, Appl. Phys. Lett. **65**, 534 (1994).
[25]L. Scheres, B. Klingebiel, J. ter Maat, M. Giesbers, H. de Jong, N. Hartmann, and H. Zuilhof, Small **6**, 1918 (2010).
[26]J. Xu, J. Drelich, and E. M. Nadgorny, Langmuir **20**, 1021 (2004).
[27]J. Xu, Y. Liao, H. D. Zheng, H. Y. Sun, J. Song, X. S. Wang, Y. Cheng, Z. Z. Xu, K. Sugioka, and K. Midorikawa, Opt. Express **15**, 12743 (2007).
[28]J. Lian, L. Wang, X. Sun, Q. Yu, and R. C. Ewing, Nano Lett. **6**, 1047 (2006).
[29]P. D. Rack, Y. Guan, J. S. Fowlkes, A. V. Melechko, and M. L. Simpson, Appl. Phys. Lett. **92**, 223108 (2008).
[30]Y. J. Oh, C. A. Ross, Y. S. Jung, Y. Wang, and C. V. Thompson, Small **5**, 860 (2009).
[31]D. Kim, A. L. Giermann, and C. V. Thompson, Appl. Phys. Lett. **95**, 251903 (2009).
[32]F. Ruffino, V. Torrisi, G. Marletta, and M. G. Grimaldi, J. Appl. Phys. **112**, 124316 (2012).
[33]F. Ruffino and M. G. Grimaldi, Appl. Surf. Sci. **270**, 697 (2013).
[34]D. Mijatovic, J. C. T. Eijkel, and A. van den Berg, Lab Chip **5**, 492 (2005).
[35]L. Libioulle, A. Bietsch, H. Schmid, B. Michel, and E. Delamarche, Langmuir **15**, 300 (1999).
[36]M. Madou, *Fundamentals of Microfabrication* (CRC Press, Boca Raton, FL, 1997).
[37]A. Kumar, H. A. Biebuyck, and G. M. Whitesides, Langmuir **10**, 1498 (1994).
[38]G. Urban, Sens. Actuators, A **74**, 219 (1999).
[39]M. A. Raza, E. S. Kooij, A. van Silfhout, H. J. W. Zandvliet, and B. Poelsema, J. Colloid Interface Sci. **364**, 304 (2011).
[40]A. A. Mewe, E. S. Kooij, and B. Poelsema, Langmuir **22**, 5584 (2006).
[41]J. Singh and J. E. Whitten, J. Phys. Chem. C **112**, 19088 (2008).
[42]S. H. Park, J. H. Im, J. W. Im, B. H. Chun, and J. H. Kim, Microchem. J. **63**, 71 (1999).
[43]D. K. Aswal, S. Lenfant, D. Guerin, J. V. Yakhmi, and D. Vuillaume, Small **1**, 725 (2005).
[44]E. Pavlovic, A. P. Quist, U. Gelius, and S. Oscarsson, J. Colloid Interface Sci. **254**, 200 (2002).
[45]K. R. Brown, L. A. Lyon, A. P. Fox, B. D. Reiss, and M. J. Natan, Chem. Mater. **12**, 314 (2000).
[46]S. M. Tabakman, Z. Chen, H. S. Casalongue, H. Wang, and H. Dai, Small **7**, 499 (2011).
[47]E. S. Kooij, E. A. M. Brouwer, H. Wormeester, and B. Poelsema, Langmuir **18**, 7677 (2002).
[48]F. Ruffino and M. G. Grimaldi, J. Nanopart. Res. **13**, 2329 (2011).
[49]*CRC Handbook of Chemistry and Physics*, edited by D. R. Lide, 86th ed. (Taylor & Francis, Boca Raton, 2005).
[50]P. B. Johnson and R. W. Christy, Phys. Rev. B **6**, 4370 (1972).
[51]E. S. Kooij, H. Wormeester, E. A. M. Brouwer, E. van Vroonhoven, A. van Silfhout, and B. Poelsema, Langmuir **18**, 4401 (2002).
[52]H. Wormeester, E. S. Kooij, and B. Poelsema, Phys. Rev. B **68**, 085406 (2003).
[53]T. W. H. Oates, D. R. McKenzie, and M. M. M. Bilek, Phys. Rev. B **70**, 195406 (2004).
[54]T. W. H. Oates and A. Mücklich, Nanotechnology **16**, 2606 (2005).
[55]R. L. Olmon, B. Slovick, T. W. Johnson, D. Shelton, S.-H. Oh, G. D. Boreman, and M. B. Raschke, Phys. Rev. B **86**, 235147 (2012).
[56]A. J. de Vries, E. S. Kooij, H. Wormeester, A. A. Mewe, and B. Poelsema, J. Appl. Phys. **101**, 053703 (2007).

Reuse of AIP Publishing content is subject to the terms at: https://publishing.aip.org/authors/rights-and-permissions. Download to IP: 130.89.45.232 On: Tue, 10 May 2016 07:25:49